Femtosecond dynamics of active semiconductor waveguides: microscopic analysis and experimental investigations

E. Gehrig and O. Hess

Advanced Technology Institute, School of Electronics and Physical Sciences, University of Surrey, Guildford, Surrey, GU2 7XH, UK

A. Volland, G. Jennemann, I. Fischer, and W. Elsäßer

Institute of Applied Physics, Darmstadt University of Technology, Schlossgartenstrasse 7, D-64289 Darmstadt, Germany

Received January 8, 2004; revised manuscript received March 30, 2004; accepted April 16, 2004

We present theoretical and experimental results of nonlinear amplification and propagation of short optical pulses in Fabry–Perot semiconductor lasers. The theoretical description is based on spatially resolved Maxwell–Bloch–Langevin equations that take into account the spatially varying light-field dynamics including counterpropagation, diffraction, self-focusing, and the microscopic carrier dynamics including carrier heating and carrier relaxation. Femtosecond pump–probe measurements using upconversion and femtosecond-resolved pump–probe measurements and frequency-resolved optical gating on a Fabry–Perot laser allow a combined analysis of the transmitted pulses in real time and the spectral domain. The experimental results are compared with the microscopically calculated gain and index distributions, pulse shapes, and optical spectra. In order to assess the full potential of semiconductor lasers and amplifiers, a quantitative measurement and understanding of amplitude and phase dynamics is required. The computer simulations of the ultrashort dynamics of semiconductor waveguides with optical injection of light pulses provide insight into the dynamic spectral gain and index changes responsible for frequency drifts and self-phase modulation, visualization of propagation effects, and a time- and frequency-resolved analysis of the amplified light pulses.

OCIS codes: 140.5960, 140.3280, 320.2250, 140.3430.

1. INTRODUCTION

The theoretical and experimental investigation of the propagation of ultrashort light pulses in active semiconductor media is of fundamental importance for the understanding of the microscopic carrier dynamics and nonlinear effects that determine the modulation response and mode stability of semiconductor lasers.[1,2] It is, in particular, spatio-spectral hole burning, carrier heating, and dynamic phase changes that affect both the spectrum and temporal shape of a light pulse during its propagation. The nonlinear light–matter coupling sets, on the one hand, an upper limit for applications, e.g., in telecommunication or nonlinear optics. On the other hand, it is of fundamental importance for the design of nonlinear elements (e.g., modulators and switches) or for the observation of nonlinear effects such as the formation of solitons.[3] With the advent of experimental femtosecond spectroscopy techniques and the development of highly mature semiconductor lasers, it is possible to experimentally investigate the ultrafast carrier dynamics in semiconductor lasers and to identify and analyze the fundamental physical effects within a microscopic theory concept that considers the underlying physical effects on a fundamental level.

Up to now, several theoretical approaches exist for the simulation of ultrashort-time effects in semiconductor lasers.[4–14] Theories on the level of the second-order Born approximation[4] explicitly take into account carrier–carrier correlations, allowing for a fundamental analysis of intra- and interband scattering effects. In this paper, we focus on the dynamic coupling between spatial, spectral, and temporal degrees of freedom occuring during the propagation of an ultrashort light pulse in a spatially extended semiconductor laser waveguide. The dynamic amplification and shaping of the light pulse is then primarily determined by the interplay of induced and spontaneous emission, counterpropagating light fields, and the spatial and spectral depletion of the carriers in the bands. In this case, it is thus important to consider the spatial, spectral, and temporal dependence of the light fields and the microscopic charge-carrier plasma within the active area. On that level of description, the carrier–carrier and carrier–phonon interaction processes can in good approximation be simulated within the frame of the relaxation-rate approximation.

We present joint theoretical and experimental studies of the nonlinear amplification and propagation of short optical pulses (~250 fs) in semiconductor lasers. The theoretical description is based on spatially resolved Maxwell–Bloch–Langevin equations, which take into account the waveguiding structure, the spatial dependence, and microscopic coupling between light and carriers in-

cluding diffraction, self-focusing, and carrier heating and relaxation through carrier–carrier and carrier–phonon scattering. The experimental studies have been performed by femtosecond pump–probe investigations on a Fabry–Perot laser by analyzing transmitted pulses both in real time and in the spectral domain using upconversion and frequency-resolved optical gating.

2. THEORY

The spatio-temporal dynamics of semiconductor laser amplifiers is determined by microscopic changes in the charge-carrier plasma, spatially dependent wave mixing between a propagating light signal and the amplified spontaneous emission and dynamic light–matter interactions leading to spatial and spectral-gain and refractive-index varations.[15] The dynamic changes in the carrier system and in the light-field distribution result from physical processes such as spatio-spectral hole burning, carrier relaxation, gain saturation, diffraction, and self-focusing. The characteristic time scales of these processes range from the femtosecond regime (fast intraband carrier relaxation) up to the picosecond and nanosecond regime (dynamics of the light fields and the spatial carrier distribution). In general, this interplay of microscopic spatio-spectral light-field and carrier dynamics within the active medium of the semiconductor laser can be described on the basis of extended Maxwell–Bloch equations (Maxwell–Bloch–Langevin equations), taking into account the spatiotemporal dynamics of the light fields, the microscopic dynamics of the charge carrier plasma in the active semiconductor, and dynamic wave-mixing processes.[16]

The dynamics of the dipole density $p^{\pm}$ [coupled to the forward (+) and backward (−) propagating optical fields] and the carrier distributions of electrons (e) and holes (h), $f^{e,h}$, is governed by the semiconductor Bloch equations

$$\begin{aligned}
\frac{\partial}{\partial t}p^{\pm}(k,r,t) &= -[i\bar{\omega}(N,T) + \tau_p^{-1}(k,N)]p^{\pm}(k,r,t) \\
&\quad - \frac{1}{i\hbar}\delta\mathcal{U}^{\pm}(k,r,t) + p_{\mathrm{fluct}}(k,r,t) \\
&\quad + \frac{1}{i\hbar}\mathcal{U}^{\pm}(k,r,t)[f^{e}(k,r,t) \\
&\quad + f^{h}(k,r,t) - 1], \\
\frac{\partial}{\partial t}f^{e,h}(k,r,t) &= g(k,r,t) + \Lambda^{e,h}(k,r,t) \\
&\quad - \gamma_{nr}f^{e,h}(k,r,t) \\
&\quad - \Gamma_{\mathrm{sp}}f^{e}(k,r,t)f^{h}(k,r,t) \\
&\quad - \sum_{\mathrm{ph}} \tau_{e,h}^{\mathrm{ph}\,-1}(k,N)[f^{e,h}(k,r,t) \\
&\quad - f_{\mathrm{eq}}^{e,h}(k,r,t,T_l)] \\
&\quad - \tau_{e,h}^{-1}(k,N)[f^{e,h}(k,r,t) \\
&\quad - f_{\mathrm{eq}}^{e,h}(k,r,t,T_{\mathrm{pl}}^{e,h})], \qquad (1)
\end{aligned}$$

with the generation rate $g(k,r,t) = (1/4\hbar)\,\mathrm{Im}[\mathcal{U}(k,r,t)^{+}p^{+*}(k,r,t) + \mathcal{U}(k,r,t)^{-}p^{-*}(k,r,t)]$, a pump term for the carrier injection $\Lambda^{e,h}(k,r,t)$, and relaxation rates for nonradiative decay (γ_{nr}) and spontaneous emission (Γ_{sp}). The scattering rates $\tau_p^{-1}(k,N)$, $\tau_{e,h}^{-1}(k,N)$ and $\tau_{e,h}^{\mathrm{ph}\,-1}(k,N)$ are microscopically calculated[17] (in dependence on wave number and carrier density) and describe carrier–carrier and carrier–phonon relaxation toward their respective quasi-equilibrium distributions $f_{\mathrm{eq}}^{e,h}(T_{\mathrm{pl}}^{e,h})$ and $f_{\mathrm{eq}}^{e,h}(T_l)$ (with carrier plasma temperature $T_{\mathrm{pl}}^{e,h}$ and lattice temperature T_l) given by the corresponding Fermi functions. At each spatial grid point and for each time step of the simulation, the appropriate value for each rate $\gamma(N,k)$ is extracted from the microscopically calculated respective parameter matrix. Typical values (depending on N and k) are 50...200 fs.

The chemical potential in the equilibrium distributions is (at every grid point) self-consistently calculated from the Fermi–Dirac functions by using the Pade approximation.[18] $\bar{\omega}$ denotes the frequency detuning between the cavity frequency and the transition frequency. It includes the bandgap renormalization $\delta\mathcal{E} = -\int_{k'}V_{k-k'}f^{e,h}(k,r,t)$ with the screened Coulomb potential $V_{k-k'}$.[19]

The propagating signal light field and the optical field arising from spontaneous emission processes within the active area together build up the local field $\mathcal{U}^{\pm}(k,r,t) = \int_{k'}d_{\mathrm{cv}}\{\mathcal{E}_{\mathrm{sig}}^{\pm}(r,t)\exp[i(k-k')r] + \mathcal{E}_{\mathrm{se}}^{\pm}(r,t)\exp[i(k-k')r]\} + \delta\mathcal{U}^{\pm}(k,r,t)$, where the spectral contributions in the sum of the light fields can be summarized in a spectral line function considering the spectral bandwidth of the injected light field and spontaneous emission, respectively. $\delta\mathcal{U}$ denotes the Coulomb-induced field contributions that are treated on the level of the Hartree–Fock approximation,[18] leading to $\delta\mathcal{U}^{\pm}(k,r,t) = -\int_{k'}V_{k-k'}p(k',r,t)$. Through the local field, the amplitude and spectral composition of the light fields and thus their spatio-spectral interference at each location within the active layer are self-consistently taken into account.

It is well known that the dynamics of semiconductor lasers is strongly affected by thermal interactions.[20,21] In our model description, we include the spatiotemporal temperature dynamics on the basis of hydrodynamic equations derived from the Boltzmann equation.[16] At every grid point, solving the hydrodynamic equations leads to spatially dependent lattice temperature and plasma temperatures (for electrons and holes). The lattice temperature enters the equations through the bandgap, while the plasma temperatures are inserted in the Fermi–Dirac equilibrium distributions for electrons and holes, respectively. Another important property is the influence of noise originating from the statistical nature of light. Incoherent noise in the light fields and dipoles gain importance when the laser is driven near threshold or in situations where a strong gain-competition exists, e.g., due to the interaction of injected light fields and amplified spontaneous emission. The lowest-order contributions are dipole–dipole and the field–field correlations that can be derived from a fully quantum-mechanical description. They can be included by adding Langevin-noise terms in

the Bloch equation of the interband dipoles and the wave equation.[22]

The dynamics of the counterpropagating optical fields $E^{\pm}$ of the injected light signal (sig) and the amplified spontaneous emission (se) yields the wave equations

$$\frac{\partial}{\partial z}E^{\pm}_{\mathrm{sig,se}}(r,\,t) \pm \frac{n_l}{c}\frac{\partial}{\partial t}E^{\pm}_{\mathrm{sig,se}}(r,\,t) = \frac{i}{2}\frac{1}{K_z}\frac{\partial^2}{\partial x^2}E^{\pm}_{\mathrm{sig,se}}(r,\,t) - \tilde{\eta}E^{\pm}_{\mathrm{sig,se}}(r,\,t) + \frac{i}{\epsilon_0}\frac{K_z}{2n_l^2}\Gamma P^{\pm}_{\mathrm{sig,se}}(r,\,t) + E_{\mathrm{fluct}}(r,\,t). \quad (2)$$

In Eq. (2), K_z denotes the wave number of the propagating fields and n_l is the refractive index of the active layer. The spatially dependent, static waveguide properties of the semiconductor laser cavity are represented by the confinement factor Γ and the complex parameter $\tilde{\eta}$, which includes the spatially dependent refractive index. $P^{\pm}$ is the polarization in the semiconductor medium, which consists, through $P^{\pm} = V^{-1}\Sigma_k d_{\mathrm{cv}} p^{\pm}$, of microscopic interband dipole densities $p^{\pm}$ (with dipole matrix element d_{cv} and carrier-momentum wave number k). E_{fluct} represents the quantum-mechanically derived light fluctuations.[22] The Langevin-noise terms, $p_{\mathrm{fluct}}(k,\,r,\,t) = (\Gamma\sqrt{2\hbar\epsilon_r})/(n_l^2 L\sqrt{\epsilon_0\omega_0})q^p(k,\,r,\,t)$ and $E_{\mathrm{fluct}}(r,\,t) = (\sqrt{\hbar\omega_0})/(\sqrt{\epsilon_r\epsilon_0})q^E r,t$, obey the correlation $\langle q^p(k,\,r,\,t)q^p(k,\,r',\,t')\rangle = \tau_p^{-1}4\pi^2$. $\{f^e(k,\,r,\,t)f^h(k,\,r,\,t) + [1 - f^e(k,\,r,\,t)][1 - f^e(k,\,r,\,t)]\}\langle q^E(r,\,t)q^E(r',\,t')\rangle = \kappa\delta(r - r',\,t - t')$, where κ describes the damping in the resonator and ω_0 is the frequency of the propagating light fields. In the simulation, the correlations are simulated with a Gaussian noise term. The optical injection of a laser signal into the semiconductor laser amplifier is taken into account through appropriate boundary conditions.[23]

For the numerical integration of the system of partial differential equations for the light fields, the Hopscotch method[24] is used as a general scheme. At every spatial location, it is self-consistently coupled and solved with the microscopic equations for the carrier and polarization Wigner distributions and the temperature equations of the lattice and the plasma. The operators are discretized by the Lax–Wendroff method.[25] Typically, 100 grid points are chosen for the x direction and 300–500 points are used for the y direction. Approximately 100–150 values are used for the discretization of the k domain.

In the following, we apply our microscopic theory to a semiconductor laser waveguide (GaAs/GaAlAs; of length 650 μm; width ~4 μm; and emission wavelength 830 nm) into which a short light pulse (width 250 fs) has been injected. The typical geometry of semiconductor laser amplifiers allows us to consider the vertical (y) direction on the basis of effective parameters. Therefore in the following we consider explicitly only field dynamics in a two-dimensional space, i.e., $r = (x, z)$. We analyze the ultrafast carrier dynamics with microscopically calculated nonequilibrium carrier distibutions of the carriers and analyze spectral gain and induced refractive index. The theoretical predictions of spectral properties are directly compared with experimental measurements. The space-dependent inclusion of the laser geometry through suitable boundary conditions and the comparative calculation and measurement of threshold current and spectral properties thereby guarantee that the numerical model exactly describes the laser used in the experiment.

3. ULTRAFAST GAIN DYNAMICS

A light pulse propagating in a semiconductor laser directly couples to the carrier populations in valence and conduction bands. Thereby it induces highly nonequilibrium distributions. As a consequence, dynamic changes in both gain and refractive index arise that relax on a time scale of a few picoseconds toward a new equilibrium distribution. Within this temporal regime, the complex dynamics of the charge carriers in combination with dynamic propagation and spatially varying light–matter coupling leads to strong distortions of the temporal and the spectral profile of the pulse.

In order to theoretically investigate the ultrafast carrier dynamics, we calculate the temporal behavior of the carrier distribution, the microscopic spectral gain, and the induced refractive index at the output facet of a semiconductor laser amplifier that has been optically excited by an ultrashort light pulse (width, 250 fs). The dynamics of the spectral gain and index can be extracted from the microscopic distribution of the dipole density [i.e., dynamically calculated within the frame work of the Bloch equations; see Eq. (1)]. The real part of the interband polarization is directly correlated to the carrier-induced spatio-spectral refractive index that the signal pulse experiences during its propagation. The imaginary part reflects the dynamics of the microscopic gain. Laterally (i.e., over the width of the active area) integrated values of these microscopic functions at the output facet consequently allow a fundamental analysis of the physical processes that are responsible for the temporal and spectral properties of an amplified light pulse. The results of the simulations are summarized in Fig. 1, depicted as Wigner distributions of the electron distribution, the microscopic gain, and the induced refractive index. Thereby we have to keep in mind that the spatial dependence of light propagation and nonlinear light–matter coupling as well as the interplay of coherent and incoherent interaction processes principally leads to a continuous mixing and partial transfer of contributions of real and imaginary part of the nonlinear interband polarization. This dynamic interplay is self-consistently included through the dynamic calculation and integration within the program code. Thus although the shown distributions are the result of a dynamic mixing of (coherent and incoherent) interaction processes, the real and imaginary part of the polarization can be interpreted as "momentary" gain and refractive index experienced for a particular time at a spatial grid point.

In the calculation, the injection current density has been set to $2.5j_{\mathrm{thr}}$ The central pulse frequency is located within the amplifier gain bandwidth so that the pulse is amplified during its propagation. The Wigner distributions show the dependence on wave number (in units of

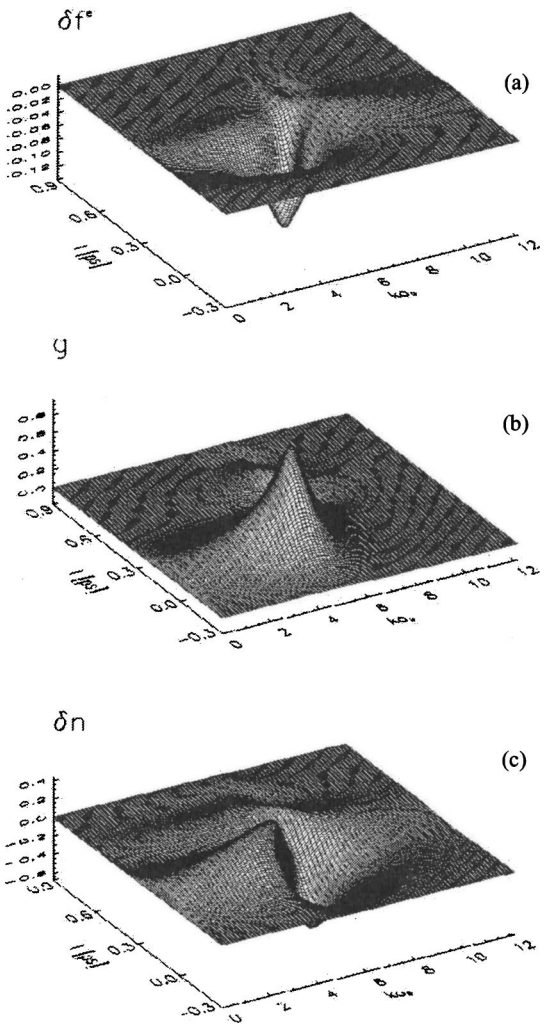

Fig. 1. Wigner distributions of (a) electrons, $\delta f^e = f^e - f^e_{\mathrm{eq}}$, (b) microscopic gain, and (c) induced refractive index at the output facet of the inverted laser amplifier during the passage of a resonant light pulse (250 fs).

the Bohr radius a_0; $k = 0$ denotes the bandgap) and on time ($t = 0$ denotes the passage of the pulse maximum through the output facet). The dynamic changes in the carrier distributions can conveniently be analyzed with the temporally and spectrally dependent deviation $\delta f^e = f^e - f^e_{\mathrm{eq}}$ from their respective equilibrium (Fermi–Dirac) distribution; here for the electrons, the hole distribution shows a qualitatively similar behavior. The calculated results for δf displayed in Fig. 1(a) visualize the physical processes that affect the spectral and temporal properties of a light pulse during its propagation: The optical excitation induced by the light pulse leads to spatio-spectral hole burning (negative values in δf) and carrier heating (positive values). The heated nonequilibrium distributions then relax through carrier–carrier and carrier–phonon scattering toward the quasi equilibrium given by the respective Fermi–Dirac distributions (where one has to insert the respective plasma temperature of electrons and holes[16]). The partial refilling of the hole through carrier relaxation and carrier injection typically occurs on time scales of a few hundred femtoseconds up to a few picoseconds. These processes consequently determine the temporal and spectral shape of the spatio-spectral trench burnt by the pulse: For high input power levels and high inversion, the spectral and temporal extension of the hole burning may thus significantly exceed the duration and spectral bandwidth of the pulse. It is this dynamic microscopic carrier response leading to a particular spectral and temporal trench in the carrier distributions that represents the physical origin of temporal and spectral distortions of the pulse. The highly nonequilibrium carrier dynamics is also reflected in the microscopic gain and induced index displayed in Figs. 1(b) and 1(c), respectively. The microscopic gain and induced index depend on the dynamics of electrons and holes in the valence and conduction bands of the semiconductor. As a consequence, they are directly affected by carrier–carrier and carrier–phonon scattering processes: The spectral hole burning and carrier heating induced by the leading part of the pulse shapes the (spectrally and temporally varying) gain [Fig. 1(b)] available for the trailing part of the pulse. At the same time, the spatio-spectral reduction of the inversion in the bands induces a dynamic spectrally dependent refractive index [Fig. 1(c)]. In particular, the reduction of the spectral inversion and the accumulation of heated-carrier states leads to a spectral broadening (reflected in the spectrally dispersive shape of the induced index) and to a temporal frequency shift (chirp). Furthermore, the dynamic carrier relaxation of the excited charge-carrier plasma leads to modulations in the trailing parts of the microscopic gain and the induced refractive index that show a characteristic drift with increasing time. The amplitude and the temporal shape of this drift are given by the carrier-injection rate (i.e., absorbing or amplification regime) and by the frequency detuning between the injected light field and the frequency of the free-running laser. The temporal dependence of gain and induced index lead to nonlinear amplification and to induced phase and frequency changes within the pulse. This self-phase modulation induced by the nonlinear interaction of a light pulse with the active semiconductor medium represents the microscopic origin for modulations (self-phase modulation) in the emission spectra observed in experiments (see below in the discussion of Fig. 3). Please note that the microscopic distributions shown are the result of the spatio-temporal integration of carrier and light-field dynamics during the pulse propagation. They are thus strongly affected by spatial variations in carrier inversion and light-field distributions. The role of these spatial effects is discussed in the following section.

4. NONLINEAR PROPAGATION EFFECTS

During the propagation of an ultrashort light pulse in a waveguide structure, the nonlinear material properties and the coupling to the transverse and longitudinal degrees of freedom of the waveguide structure determine the spatio-temporal light-field dynamics. Next to the geometrical influences, it is in particular the nonlinear gain saturation and index changes that lead to a reshaping and a temporal broadening of the propagating light pulse. The saturation behavior thereby depends on a variety of physical interactions whose traces can be found in both space and frequency domains: The fast microscopic

interactions (typical time scales being a few 100 fs) in the charge-carrier plasma, e.g., spatio-spectral hole burning, carrier heating, and spatio-spectral wave mixing between the propagating light pulse and the amplified spontaneous emission, are responsible for a time-dependent phase shift between the microscopic gain and induced index (see Section 3) that lead to fast self-phase modulation. The slow macroscopic changes are the long-lived reduction of the carrier density in the active area leading to spatial gain and index profiles. Both the slow and fast phase changes result in distortions of the pulse shape, spectral broadening, and inference effects in the optical spectrum. It is important to note that these spatial, spectral, and temporal changes are the result of a continuous interaction between light and matter during the propagation of the pulse. Thus they cannot be appropriately described if spatial dependencies and variations of the light fields and the carriers are neglected, as in the case of spatially averaged simulations.

In order to visualize the spatio-temporally varying light propagation, we calculate the laser internal intensity distribution during the propagation of an ultrashort light pulse in an inverted ($j = 2.5j_{\mathrm{thr}}$) semiconductor waveguide (length 650 μm). Figure 2 shows temporal snapshots of the intensity taken in the (a) front, (b) middle, and (c) back part of the active area during the propagation of a light pulse (with energy 27 pJ and duration 250 fs). Note that only the spatial region around the respective pulse position, and not the entire active area, is plotted. The snapshots visualize the influence of the microscopic amplification, saturation, and induced index dynamics on the signal amplification. During its propagation in the waveguide structure the pulse, through its nonlinear continuous interaction with the microscopic charge-carrier plasma, is significantly reshaped. The leading part of the pulse experiences the initial gain, whereas the trailing part experiences a gain that has been significantly reduced by the leading part. As a consequence, the trailing part of the pulse is less amplified than the leading part, resulting in a steep rise in the front part and a significant broadening of the pulse in the propagation direction. The intensity variations in the transverse direction are determined by spatial gain and index profiles induced by the pulse during propagation, leading to dynamic self-focusing: The guiding of the light fields leads in the lateral center of the laser cavity to a stronger depletion of the inversion. As a consequence, that spatial gain that is defined through $G(r, t) = -\int_k g(k, r, t)$ is high in the transverse center and decreases toward the edges. At the same time, the induced recombination leads to an increase in refractive index. In combination, the spatial-gain and refractive-index dynamics lead to dynamic self-focusing that counteracts the diffraction of the light fields. Additionally, the dynamic coupling of longitudinal with transverse degrees of freedom induces through carrier scattering, diffusion, and light diffraction a partial transfer of longitudinal variations in gain and index to transverse variations, leading to characteristic transverse modulations within the pulse shape [see Fig. 2(c)]. During its propagation in the waveguide, the light pulse not only reduces the spatial inversion but also induces a dynamic excitation of carriers in the bands leading to spectral hole burning and carrier heating. The carrier thermalization following the pulse-induced excitation of the medium causes a partial reestablishment of the spectral gain. It is these time-depending gain changes that may result in characteristic modulations that can be seen in Fig. 2(c).

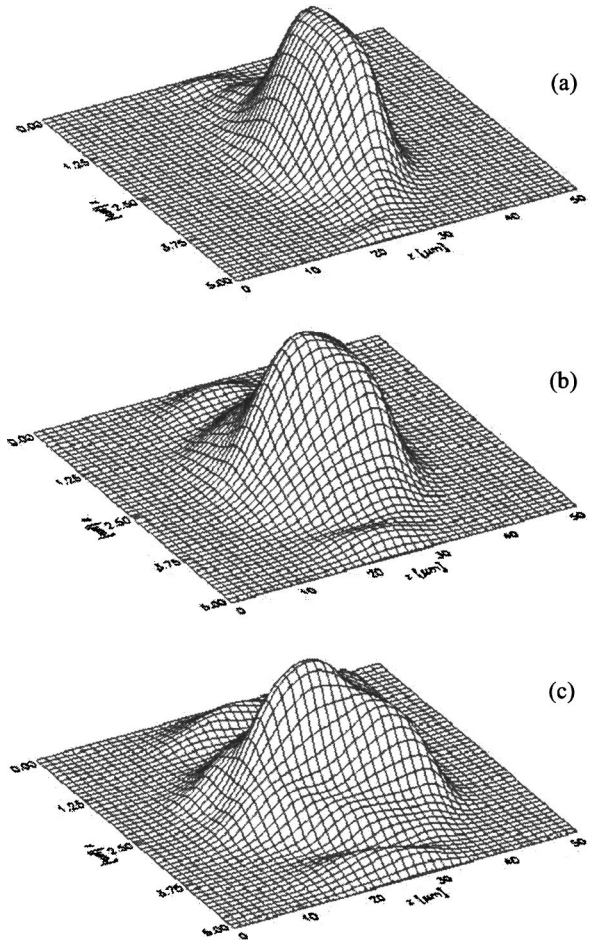

Fig. 2. Intensity snapshots of the propagating pulse after passing (a) one third, (b) two thirds, and (c) the entire length of the semiconductor laser amplifier.

The nonlinear amplification and dynamic reshaping of the pulse consequently is the result of both spatial variations (in gain and index) and ultrafast changes occurring during the propagation in the spatially dependent charge-carrier plasma. Thereby it is, in particular, the coupling of spatial with spectral degrees of freedom that determines amplitude and phase of the pulse. The spatio-temporally varying light–matter coupling not only affects the shape of the propagating pulse, but also its spectral properties. The spatio-spectral reduction of the carrier inversion leads to a partial spatio-spectral gain saturation and to induced changes of the instantaneous refractive index.[26] The resulting retardation and acceleration of the light-field contributions within the pulse envelope cause dynamic phase changes that lead to chirping within the pulse. The spatio-temporal superposition of field contributions belonging to the individual frequencies may interfere, thereby causing modulations in the spectrum (self-phase modulation).

Figure 3 shows calculated optical spectra of a propagat-

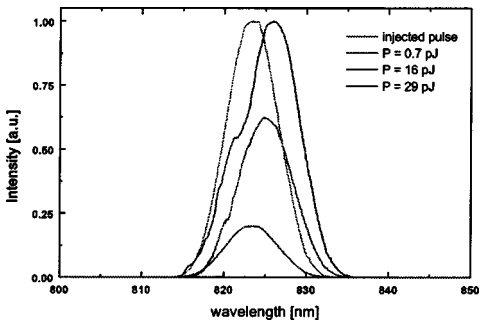

Fig. 3. Calculated spectra of the amplified pulse after propagation in the semiconductor laser amplifier for pulse energies of 0.7 pJ, 16 pJ, and 29 pJ (from bottom to top). For comparison, the original pulse spectrum (corresponding to a wavelength of 823.5 nm.) is included.

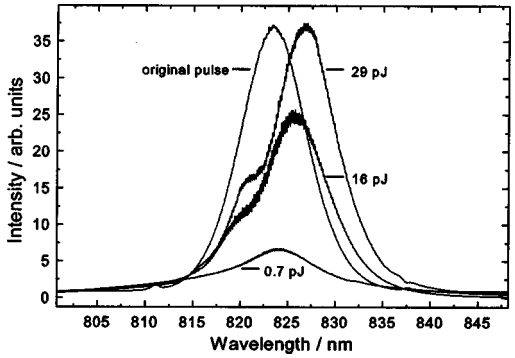

Fig. 4. Experimental spectra correponding to the theoretical spectra of Fig. 3. Pulse energies are, from bottom to top, 0.7 pJ, 16 pJ, and 29 pJ; the original pulse spectrum corresponds to a wavelength of 823.5 nm.

ing light pulse in comparison to the spectrum of the injected light pulse. Shown are spectra for three different pulse energies. The injection current is 50 mA. Figure 4 displays the corresponding experimental result. The theoretical model predicts spectral broadening and the generation of a second peak on the short-wavelength side of the main peak. When the propagating light pulse saturates the amplifier, the spatio-spectral inversion is significantly reduced by the leading part of the pulse. The spatio-spectral hole burning and carrier heating induced by the pulse in the charge-carrier plasma leads, through the interband polarization, to a reduction of the microscopic spectral gain (which is then partially reestablished by carrier thermalization) and to an increase of the spatio-spectral refractive index. In addition to these fast (femtosecond and picosecond) gain and index dynamics, the pulse significantly reduces the spatially dependent total carrier density. This effect leads to slow, long-lived changes in the local gain and refractive index on a time scale of a few hundred picoseconds. Saturation of the gain and induced index dispersion together lead to a spectral broadening and a spectral shift of the central wavelength of 3.3 nm. The spatio-spectral gain and index distributions determine amplitude and phase, as well as the spectral properties of the propagating light pulse: The temporal variations of the nonlinear phase ϕ created by the slow and fast changes in the carrier system is related to respective frequency variations through $\delta\omega \propto -\dot{\phi}$. As a consequence, a frequency may appear twice within the pulse envelope. The interference of the optical field contributions at the individual frequencies with their respective relative phase then determines the spectral width and leads, for high injection current and high pulse energies, to a characteristic modulated shape in the observed optical emission spectrum (self-phase modulation[27]). The asymmetric pulse envelope resulting from the gain saturation thereby directly reflects the asymmetry of the optical spectrum. The close agreement between theory and experiment demonstrates (1) that the model description can confirm, without using any fit parameters, experimental measurements and (2) the "look inside the laser," e.g., the fundamental analysis of, e.g., microscopic carrier distributions and laser internal intensity distributions that through the nonlinear light–matter coupling result in a particular spectrum directly representing the experimental situation. Spectral broadening and self-phase modulation that can be observed in experiments are thus the result of microscopic spatially dependent carrier dynamics that arise during the propagation of a light pulse. However, these nonlinear effects not only limit the signal transmission but may also be advantageous for specific applications of nonlinear effects, e.g., solitons.[3]

5. DYNAMIC SPECTRAL PROPERTIES

A direct experimental access to ultrafast nonlinear effects in semiconductor lasers can be obtained through pump–probe measurements.[6,13,28–31] This allows both the analysis of the temporal properties of a propagating pulse (i.e., its pulse shape and width) and the spectral properties through a frequency-resolved optical-gating technique[32] (FROG). The second-harmonic generation FROG technique used in this paper has the advantage of an increased sensitivity compared with FROG techniques based on χ^3 processes.[30,33] A sketch of the experimental pump–probe setup is shown in Fig. 5. The light pulses (duration ~250 fs) generated by a Ti:sapphire laser are divided into two pulses of different intensity and polarization: an intense pump pulse and a weak probe pulse. The two pulses are delayed with respect to each other in a Michelson interferometer and are then injected into the active area of the Fabry–Perot semiconductor laser. The transmitted probe pulse signal is phase-sensitively detected with a photodiode and a lock-in amplifier. This transmitted probe signal through the semiconductor laser reflects all relaxation mechanisms and coherent effects in the charge-carrier plasma of the laser. The microscopic calculation of the Wigner functions of the carriers and the interband polarization allows one to directly extract the frequency- and time-dependent light-field contributions through the local fields $U(k, r, t)$. Converting the k scaling through $k = 2\pi/\lambda$ into a wavelength scale leads to λ- and time-dependent distributions that can be directly compared with the experimental FROG plot. The simulation of a reference pulse is not required since the spatially and temporally resolved model allows one to directly monitor the light-field contributions and micro-

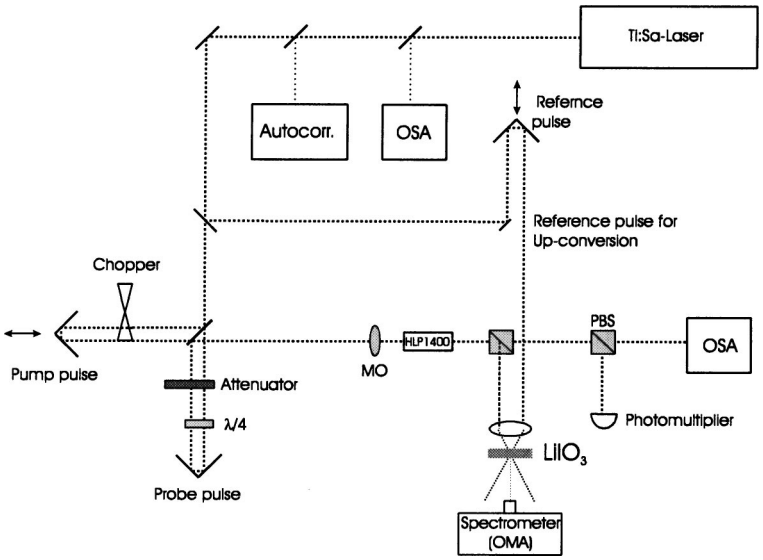

Fig. 5. Experimental setup of the pump–probe experiment.

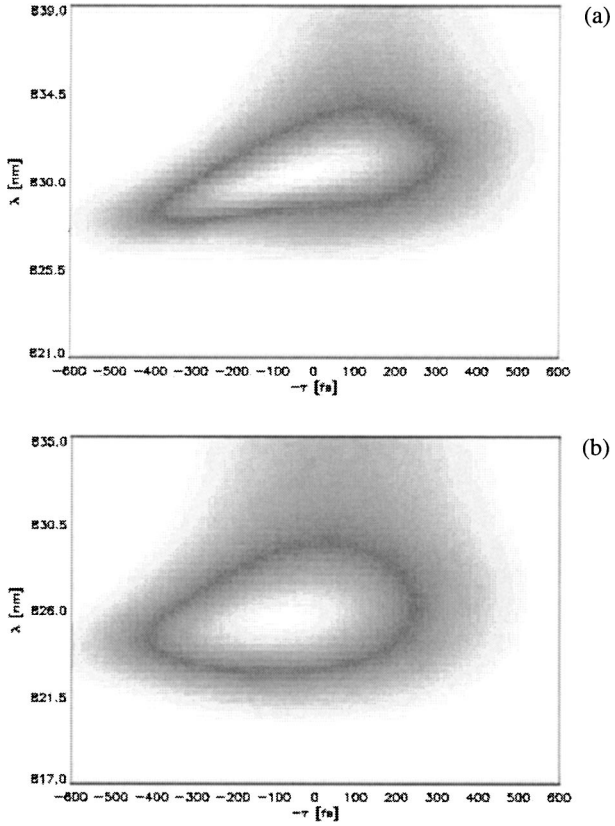

Fig. 6. Calculated FROG plots with 30-pJ excitation energy. The injection current is 50 mA, and the wavelength is (a) 830 nm and (b) 825 nm.

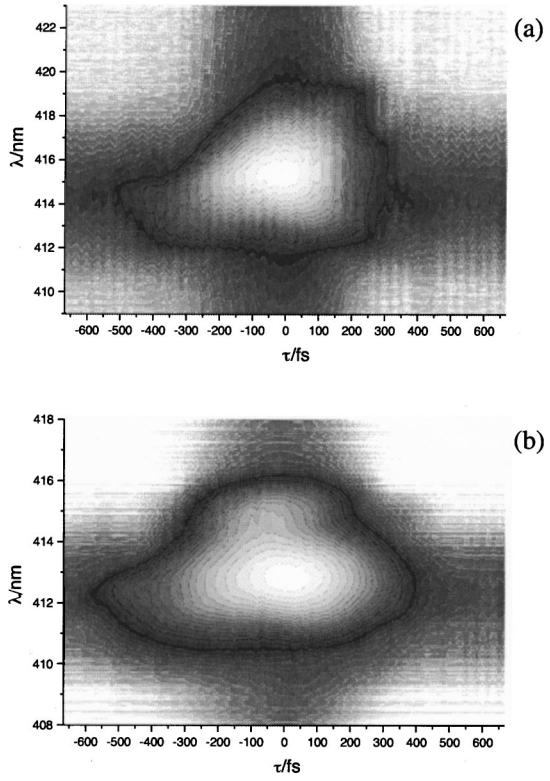

Fig. 7. Experimental FROG plots with 30-pJ excitation energy. The injection current is 50 mA, and the wavelength is (a) 830 nm and (b) 825 nm.

scopic distributions for every time step and frequency component within the pulse envelope. In the experimental investigation, a reference pulse is required in order to perform a stepwise scanning of the distributions for different times within the pulse shape. The calculated spectral composition of the light fields in each temporal slice within the pulse shape can then be compared directly to the experimental FROG plot.

Figures 6 and 7 display calculated (Fig. 6) and measured (Fig. 7) FROG plots. The semiconductor laser has been driven at its threshold injection current; the pulse energy of the pump pulse is 30 pJ. For a better visualization, a logarithmic three-color scale has been chosen, with white indicating very high and very low intensity. Black represents the intermediate regime. In Figs. 6(a) and 7(a), the wavelength of the pump pulse has been set to 830 nm, corresponding to the gain maximum of the laser. One can see that the gain saturation generated by

the resonant pulse leads to a steep rise and through the induced index changes, to the generation of new frequencies and consequently to a broadening of the spectrum in the leading part. Owing to the carrier-induced increase of the instantaneous index, the spectrum at the red side of the maximum is much broader than on the blue side, leading to an overall redshift in the pulse center. The drift of approximately 0.7 nm of the spectral maximum that can be observed in the time interval between $-\tau = 300$ fs and $-\tau = 0$ fs can be attributed to the instantaneous negative refractive-index changes in the trailing-pulse part. In particular, Figs. 6(a) and 7(a) clearly show a blueshift of approximately 1 nm of the central wavelength in the trailing part of the pulse between -200 fs and -400 fs. This effect demonstrates the influence of carrier thermalization on the refractive index. In Figs. 6(b) and 7(b), the wavelength of the pump pulse has been set to 825 nm. This leads to a completely different behavior. The blueshift in the trailing part of the pulse is much weaker than in the situation displayed in the upper diagram. In addition, the spectrum in the leading part of the pulse is less broadened. The good agreement between theory and experiment shows that the spatially and spectrally resolved simulation on the basis of a Maxwell–Bloch–Langevin description allows a microscopically based interpretation and visualization of the complex ultrashort light–matter interactions that influence the spatio-temporal dynamics of semiconductor laser waveguides. In the shown example, these are, in particular, nonlinear spatially varying light propagation, inhomogeneous gain saturation, and microscopic carrier dynamics leading to hole burning, carrier heating, and relaxation. We would like to note that the simulation of high-nonequilibrium conditions, e.g., a strongly off-resonant injection of a very intense ultrashort light pulse, would require a more detailed inclusion of carrier-scattering mechanisms.[13] However, our model description has the advantage that it allows the simultaneous calculation of spatial and spectral dependencies. This is of particular importance for the description of spatially extended lasers (e.g., large transverse width and/or long propagation lengths of several 100 μm), where counter-propagation and the transverse dependence of the optical fields play an important role.

6. CONCLUSION

We have investigated the spatio-temporal light-field dynamics and the ultrafast carrier dynamics in active semiconductor laser waveguides. Experimental results of the dynamically resolved spectral properties obtained with a pump–probe setup have been analyzed within the frame work of a spatially resolved Maxwell–Bloch–Langevin description. Results from computer simulations show that, in particular for long propagation lengths, it is the dynamic coupling between the longitudinal and transverse degrees of freedom characterized by spatio-spectral gain saturation, refractive-index dynamics, light diffraction, and microscopic carrier scattering that affects a light pulse propagating in a semiconductor laser waveguide.

REFERENCES

1. G. P. Agrawal and N. K. Dutta, *Long Wavelength Semiconductor Lasers* (Van Nostrand Reinhold, New York, 1986).
2. See, e.g., G. P. Agrawal and N. K. Dutta, *Semiconductor Lasers* (Van Nostrand Reinhold, New York, 1993), and references therein.
3. E. Gehrig and O. Hess, "Propagating spatial optical solitons in semiconductor lasers," Opt. Photonics News **10**(12), 23–25 (1999).
4. A. Knorr and S. Hughes, "Microscopic theory of ultrashort pulse compression and break-up in a semiconductor optical amplifier," IEEE Photonics Technol. Lett. **13**, 782–784 (2001).
5. J. F'orstner, A. Knorr, and S. W. Koch, "Nonlinear pulse propagation in semiconductors: hole burning within a homogeneous line," Phys. Rev. Lett. **86**, 476–479 (2001).
6. T. Meier, S. W. Koch, P. Brick, C. Ell, G. Khitrova, and H. M. Gibbs, "Signature of correlations in intensity-dependent excitonic absorption changes," Phys. Rev. B **62**, 4218–4221 (2000).
7. A. Thranhardt, S. Kuckenberg, A. Knorr, P. Thomas, and S. W. Koch, "Interplay between coherent and incoherent scattering in quantum well secondary emission," Phys. Rev. B **62**, 16802–16807 (2000).
8. A. Thranhardt, C. Ell, S. Mosor, G. Rupper, G. Khitrova, H. M. Gibbs, and S. W. Koch, "Interplay of phonon and disorder scattering in semiconductor quantum wells," Phys. Rev. B **68**, 035316 (2003).
9. W. Hoyer, M. Kira, and S. W. Koch, "Influence of Coulomb and phonon interaction on the exciton formation dynamics in semiconductor heterostructures," Phys. Rev. B **67**, 155113 (2003).
10. J. Li and C. Z. Ning, "Hydrodynamic theory for spatially inhomogeneous semiconductor lasers. I. A microscopic approach," Phys. Rev. A **66**, 023802 (2002).
11. H. G. Breunig, T. Voss, I. Ruckmann, J. Gutowski, V. M. Axt, and T. Kuhn, "Influence of higher Coulomb correlations on optical coherent-control signals from a ZnSe quantum well," J. Opt. Soc. Am. B **20**, 1769–1779 (2003).
12. J. V. Moloney, R. A. Indik, J. Hader, and S. W. Koch, "Modeling semiconductor amplifiers and lasers: from microscopic physics to device simulation," J. Opt. Soc. Am. B **16**, 2023–2029 (1999).
13. S. Hughes, P. Borri, A. Knorr, F. Romstad, and J. M. Hvam, "Ultrashort pulse-propagation effects in a semiconductor optical amplifier: microscopic theory and experiment," IEEE J. Sel. Top. Quantum Electron. **7**, 694–702 (2001).
14. R. A. Indik, J. V. Moloney, R. Binder, A. Knorr, and S. W. Koch, "Self-induced channeling of subpicosecond optical pulses in broad-area bulk semiconductor amplifiers," Opt. Lett. **20**, 2315–2317 (1995).
15. E. Gehrig and O. Hess, "Spatio-temporal dynamics of light amplification and amplified spontaneous emission in high-power tapered semiconductor laser amplifiers," IEEE J. Quantum Electron. **37**, 1345–1355 (2001).
16. E. Gehrig and O. Hess, "Nonequilibrium spatio-temporal dynamics of the Wigner distributions in broad-area semiconductor lasers," Phys. Rev. A **57**, 2150–2162 (1998).
17. O. Hess and T. Kuhn, "Maxwell–Bloch equations for spatially inhomogeneous semiconductor lasers. I: Theoretical description," Phys. Rev. A **54**, 3347–3359 (1996).
18. W. W. Chow, S. W. Koch, and M. Sargent III, *Semiconductor-Laser Physics* (Springer-Verlag, Berlin, 1994).
19. M. Lindberg, R. Binder, and S. W. Koch, "Theory of the semiconductor photon echo," Phys. Rev. A **45**, 1865–75 (1992).
20. A. Uskov, J. Mørk, and J. Mark, "Wave mixing in semiconductor laser amplifier due to carrier heating and spectral hole burning," IEEE J. Quantum Electron. **30**, 1769–1781 (1994).
21. P. O'Brien, J. O'Callaghan, and J. McInerney, "Internal temperature distribution measurements in high power semiconductor lasers," Electron. Lett. **34**, 1399–1401 (1998).

22. H. F. Hofmann and O. Hess, "Quantum Maxwell–Bloch equations for spatially inhomogeneous semiconductor lasers," Phys. Rev. A **59**, 2342–2358 (1999).
23. E. Gehrig, D. Woll, M. Tremont, A. Robertson, R. Wallenstein, and O. Hess, "Saturation behavior and self-phase modulation of picosecond pulses in single-stripe and tapered semiconductor laser amplifiers," J. Opt. Soc. Am. B **17**, 1452–1456 (2000).
24. I. S. Grieg and J. D. Morris, "A Hopscotch method for the Korteweg–de Vries equation," J. Comput. Phys. **20**, 60–84 (1976).
25. W. H. Press, B. P. Flannery, S. A. Teukolsky, and W. T. Vetterling, *Numerical Recipes* (Cambridge University, Cambridge, UK, 1989).
26. K. L. Hall, G. Lenz, A. M. Darwish, and E. P. Ippen, "Subpicosecond gain and index nonlinearities in InGaAsP diode lasers," Opt. Commun. **111**, 589–612 (1994).
27. G. P. Agrawal and N. A. Olsson, "Self-phase modulation and spectral broadening of optical pulses in semiconductor laser amplifiers," IEEE J. Quantum Electron. **25**, 2297–2306 (1989).
28. K. L. Hall, G. Lenz, E. P. Ippen, and G. Raybon, "Heterodyne pump probe technique for time-domain studies of optical nonlinearities in wave-guides," Opt. Lett. **17**, 874–876 (1992).
29. P. Borri, W. Langbein, J. Mørk, and J. M. Hvam, "Heterodyne pump–probe and four-wave mixing in semiconductor optical amplifiers using balanced lock-in detection," Opt. Commun. **169**, 317–324 (1999).
30. F. Romstad, P. Borri, W. Langbein, J. Mørk, and J. M. Hvam, "Measurement of pulse amplitude and phase distortion in a semiconductor optical amplifier: from pulse compression to breakup," IEEE Photonics Technol. Lett. **12**, 1674–1676 (2000).
31. M. Hofmann, S. Brorson, J. Mørk, and A. Mecozzi, "Subpicosecond heterodyne four-wave mixing experiments on InGaAsP semiconductor laser amplifiers," Opt. Commun. **139**, 117–124 (1997).
32. http://www.physics.gatech.edu/gcuo/Tutorial/tutorial.html.
33. K. W. DeLong, R. Trebino, J. Hunter, and W. E. White, "Frequency-resolved optical gating with the use of second-harmonic generation," J. Opt. Soc. Am. B **11**, 2206–2215 (1994).